

Surface-edge state and half quantized Hall conductance in topological insulators

Rui-Lin Chu,¹ Junren Shi,² and Shun-Qing Shen¹

¹*Department of Physics and Center of Computational and Theoretical Physics,
The University of Hong Kong, Pokfulam Road, Hong Kong*

²*International Center for Quantum Materials, Peking University, Beijing 100871, China*
(Dated: September 15, 2018)

We investigate the transport properties of the surface states of a three-dimensional topological insulator in the presence of a spin-splitting Zeeman field. We propose a picture that the chiral edge state forms on the surface, and is split into two halves that are spatially separated, each carrying one half of the conductance quantum (e^2/h). This picture is confirmed by numerical simulation in a four-terminal setup. It is demonstrated that the difference between the clockwise and counterclockwise transmission coefficients of the two neighboring terminals is approximately one half, which suggests that the half quantized Hall conductance can be manifested in an appropriate experimental setup.

PACS numbers: 73.20.-r; 73.43.-f

Topological insulators are insulating in the bulk, but have metallic surface states possessing an odd number of Dirac cones of massless fermions [1–3]. The band structure and the quantum spin texture of these surface states have been well established theoretically and experimentally [4–9]. In the presence of a spin-splitting Zeeman field, which could be induced by magnetically doping the samples or putting the samples in the proximity of ferromagnetic materials, the Dirac fermions will gain a mass and the spectrum opens a gap [10, 11]. When the Fermi level is located within the energy gap, it was proposed that the Hall conductance of the surface states will be one half of the conductance quantum e^2/h [12–14]. Based on this, Qi et al. proposed the unconventional magnetoelectric effect, which is regarded as one of the characteristic features of the topological insulators [14–16].

On the other hand, it is not clear whether or not the half quantization of the Hall conductance can be directly observed in the transport measurement. In the usual quantum Hall system, the current-carrying chiral edge states are responsible for the integer quantized Hall conductance measured in the transport experiment.[17, 18] It is not immediately clear whether or not the similar chiral edge state will form on the closed surface of a topological insulator, and how the quantized nature of the edge states can be reconciled with the prediction of the half quantization of the Hall conductance.[12–14]

To get a definite answer to these questions, we investigate the multi-terminal transport properties of a 3D topological insulator in the presence of a uniform spin-splitting Zeeman field. We propose that the closed surface of the topological insulator will form two insulating domains of the different topologies (i.e., positive vs. negative gaps), separated by a gapless metallic belt. A chiral edge state will form and is concentrated around the boundaries between the insulating domains and the metallic belt. Effectively, the chiral edge state is split into two halves, each of which is circulating around the boundary of one of the domains and carrying one half of

the conductance quantum (e^2/h). Such a picture reconciles the apparent conflict between the half quantization and the index theorem. It also suggests that by attaching the electrodes to the boundary of one of these domains, it is possible to directly measure the half quantized Hall conductance. The picture as well as its prediction are verified by the numerical simulation based non-equilibrium Green's function method.

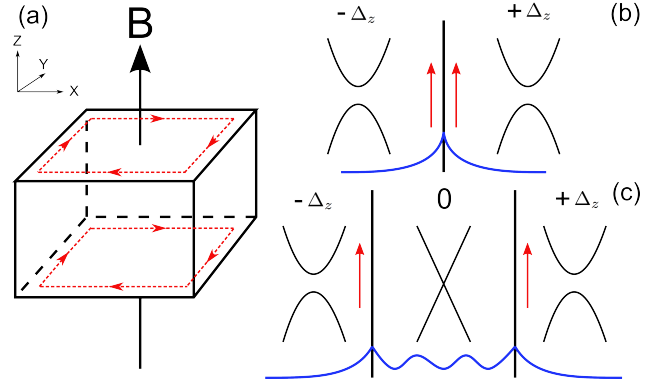


FIG. 1: (Color online) (a) Schematic of a 3D TI in a weak Zeeman field, and the formation of chiral current on the top and bottom surface boundaries. (b) A chiral edge state will form around the domain wall between the 2D Dirac fermions with positive and negative masses, and the wave function is illustrated. The arrow indicates the flow of edge current. (c) When the sharp domain wall evolves to finite-width metallic band, the edge mode is effectively split to two halves concentrated around the two boundaries.

To illustrate the basic physics, we consider a 3D topological insulator of the cubic shape. A Zeeman field is applied along the z -direction, as shown in Fig. 1(a). Because the bulk of the system is insulating, it is effectively a closed 2D surface with six facets. The effective Hamiltonian of the Dirac fermions for the surface state can be written as [19, 20]:

$$H_{\text{eff}}(\mathbf{k}) = v(\mathbf{k} \times \boldsymbol{\sigma}) \cdot \mathbf{n} - g_{\parallel} \mu_B \hbar \sigma_{\parallel} - g_{\perp} \mu_B \hbar \boldsymbol{\sigma}_{\perp} \cdot \boldsymbol{\sigma}_{\perp}, \quad (1)$$

where \mathbf{n} denotes the normal vector of the surface, $\boldsymbol{\sigma} \equiv \{\sigma_x, \sigma_y, \sigma_z\}$ are the Pauli matrices, $h_{\parallel} (\sigma_{\parallel})$ and $\mathbf{h}_{\perp} (\boldsymbol{\sigma}_{\perp})$ are the Zeeman field (Pauli matrix) components parallel and perpendicular to the normal vector, respectively, and g_{\parallel} and g_{\perp} are the corresponding spin g -factor. Note that the surface state has the anisotropic spin g -factor due to the strong spin-orbit coupling of the bulk band: g_{\parallel} is the same as the g -factor of the bulk material, and g_{\perp} is renormalized by bulk band parameters and is usually strongly suppressed [19, 20]. The different facets of the surface have the different effective Hamiltonians respective to the different normal vectors \mathbf{n} . For the top and the bottom facets, the effective Hamiltonian can be written as $H_{\text{eff}} = \pm v(k_x \sigma_y - k_y \sigma_x) + \Delta_z \sigma_z$, where $+$ and $-$ are for the top and bottom surfaces, respectively, and $\Delta_z \equiv -g_{\parallel} \mu_B h$. The spectrum will open a gap on these facets, and the Dirac fermions gain a mass $\pm \Delta_z$. On the other hand, the effective Hamiltonians for the side facets can be written as the forms like $H_{\text{eff}} = v[(k_x + \Delta k) \sigma_z - k_x \sigma_x]$, where $\Delta k \equiv g_{\perp} \mu_B h$. In this case, the Zeeman field has no effect except shifting the Dirac point. When the Fermi level is located in the gap of the top and bottom surface, the system becomes effectively two insulating domains separated by a conducting belt with massless Dirac fermions.

The two insulating domains belong to the different topological classes due to the fact that the normal vectors for the top and the bottom surfaces are in the opposite directions. We consider the limiting case that the sample has the vanishing thickness along the z -direction (but ignore the coupling between the top and bottom surfaces). The system is locally equivalent to a domain-wall structure across which the Dirac fermion masses changes from positive to negative, as shown in Fig. 1(b). The change of the band topology necessitates the close of the energy gap around the domain wall, giving rise to the gapless edge mode. By directly solving the wave equation and matching the wave functions at the boundary, it is easy to obtain that the wave function of the edge mode has the form $\Psi(x, y) = \sqrt{\Delta_z/4\pi v}(1, 1)^T \exp[-(\Delta_z/v)|x| + ik_y y]$, and the dispersion is linear in the momentum: $E = -vk_y$. The edge mode will form an ideal one-dimensional chiral edge channel carrying a quantized conductance e^2/h . The channel cannot be backscattered and is robust against the disorder. Transport measurement will yield a quantized Hall conductance if attaching electrodes to the edge of the sample.

When the thickness of the sample along the z -direction is finite, the two insulating domains are separated by a finite metallic region of massless Dirac fermion, equivalent to the configuration shown in Fig. 1(c). In this case, the electrons in the metallic region will in general form sub-bands due to the confinement by the insulating domains. The normal sub-band has dispersion $E_n = \pm v \sqrt{k_y^2 + k_n^2}$, where $k_n \neq 0$ is one of the discrete

momentums of the eigen-modes along the confinement direction. Beside these, there is a chiral solution with the dispersion $E = -vk_y$, corresponding to $k_n = 0$ but with only the left-going mode. The chirality is also shown in the penetration amplitude of the normal sub-band wave function into the insulating domains: the penetration amplitude maximizes when $E \sim -vk_y$, and decreases when moving away from it. All sub-bands crossing the Fermi energy will contribute to the transport properties, and form a novel chiral edge state as a result of collective combination (not a single mode). The chirality will give rise to a finite Hall conductance.

To see what the transport measurement will yield for such a system, we employ the direct numerical simulation. We investigate an isotropic 3D topological insulator with the tight-binding Hamiltonian on a cubic lattice:

$$\mathcal{H} = \sum_i c_i^\dagger \mathcal{M}_0 c_i + \sum_{i,\alpha=x,y,x} \left(c_i^\dagger \mathcal{T}_\alpha c_{i+\alpha} + c_{i+\alpha}^\dagger \mathcal{T}_\alpha c_i \right) \quad (2)$$

where $\mathcal{T}_\alpha = B\sigma_z \otimes \sigma_0 - i\frac{A}{2}\sigma_x \otimes \sigma_\alpha$ and $M_0 = (M - 6B)\sigma_z \otimes \sigma_0 + \Delta_z \sigma_0 \otimes \sigma_z$. The lattice space is taken to be unity. Near the Γ point in the k space, it is reduced to a Dirac-like model, which can be derived from either the theory of invariants [7], or the 8-band extended Kane model near the inversion of the Γ_6^- and Γ_8^+ bands. The Dirac model for a topological insulator has been discussed by several authors [14, 21]. It was shown that the model yield the effective surface Hamiltonian Eq. 1 with $v = A$ [19, 20]. We first employ the Green function technique to calculate the local density of states (LDOS) for the surface states, in particular the spatial distribution near the boundary, to demonstrate the formation of the edge state. Then we calculate the Hall conductance for a four-terminal setup, which directly reflects the output of the transport measurement.

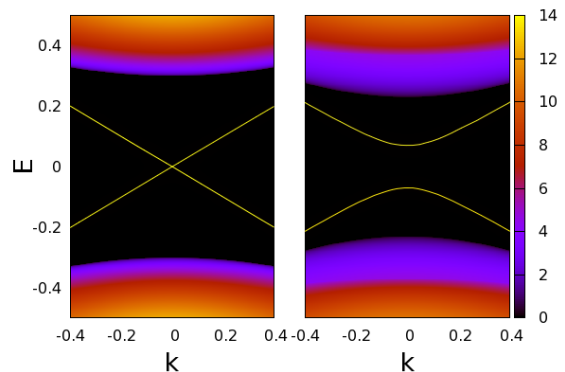


FIG. 2: (Color online) Local density of state on an infinite surface of a semi-infinite 3D system. (left) gapless single Dirac cone of the surface state; (right) gap opening by application of a Zeeman splitting term. The model parameters are $A = 0.5$, $B = 0.25$, $M = 0.3$, and $\Delta_z = 0.07$.

In Fig.2 we present LDOS $\rho(k_x, k_y)$ of the top surface for a semi-infinite sample with $z \in [0, -\infty)$. In this case,

k_x and k_y are good quantum numbers. A recursive approach are employed to calculate the Green's function for a few top layers [22]. LDOS at the top surface can be calculated by $\rho_i(k_x, k_y) = -\frac{1}{\pi} \text{Tr}[\text{Im}G_{ii}(k_x, k_y)]$, where G_{ii} is the retarded green function for the i th layer from the top. In the absence of the Zeeman field, the gapless linear Dirac cone can be observed. Position dependence of LDOS along the z -axis shows that the states in the Dirac cone reside dominantly near the top surface, which is characteristic of the surface states for a topological insulator, and is consistent with the analytical solution.[19] In the presence of the Zeeman field, the LDOS shows that a gap of magnitude $2\Delta_z$ is opened, as expected.

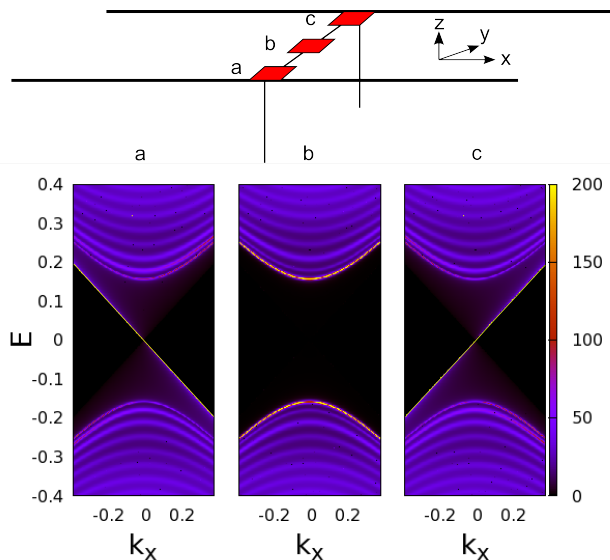


FIG. 3: (Color online) LDOS on the top surface of a structure that is infinite in X, finite in Y and semi-infinite in Z direction. Sampling is taken correspondingly in a, b and c regions as illustrated in the upper panel. $\Delta_z = 0.15$, $M = 0.4$, and $L_y = 30a$ (a is the lattice space).

To see the distribution of the surface states near the edge of the top surface, we study a geometry that is finite in the y axis, infinite in the x axis and semi-infinite in the z axis, as illustrated in the upper panel of Fig. 3. In this case only k_x is a good quantum number. The LDOS is $\rho(y, k_x) = -\frac{1}{\pi} \text{Tr}[\text{Im}G_{00}(y, k_x)]$. The average LDOS at three small different regions (a)–(c) along the y -direction are shown in the lower panel of Fig.3. It can be seen that the finite density of states emerges in the gap at the locations (a) and (c) near the boundaries of the top surface. The finite density of the in-gap states originates from the penetrated wave functions from the side facets, which will decay exponentially in space when the energy of the state is located in the gap of the top surface states. The chiral nature of these in-gap states can be directly observed: the LDOS at the edge (a) maximizes at $E = -v k_x$ (left going), while the LDOS at the edge (c) maximizes at $E = v k_x$ (right going). As a result,

these states will carry a net chiral edge current.

We calculate the current density profile of these in-gap states at the fermi surface E_f along the y -direction using $\langle J_x(y) \rangle = ie \int_{k_x} \text{Tr}[v_x(r, k_x) G^<(r, k_x)]$ where $v_x = \partial H / \partial k_x$ is the velocity operator and E_f is in the Zeeman splitting gap. In an equilibrium condition we have $G^< = f(E_f)(G^a - G^r)$, where $f(E_f)$ is the Fermi-Dirac distribution function and we assume zero temperature. In Fig. 4a the current density distribution along the y -direction for the top five layers is shown. It can be seen that the current is localized dominantly near the edges in the insulating top layers. To see the distribution of the chiral edge current in the side facets, we sum up the current density for each layer over the half the width of y : $J_t = \sum_0^{L_y/2} J_x(y)$ and observe its layer dependence. As is shown in Fig. 4b, J_t shows the typical behavior of Friedel oscillation [23], which maximize at the boundary and decays to zero when moving away from the boundary. We see that the distribution of the chiral edge current is concentrated around the boundary, even the wave-functions in the metallic region are all extended.

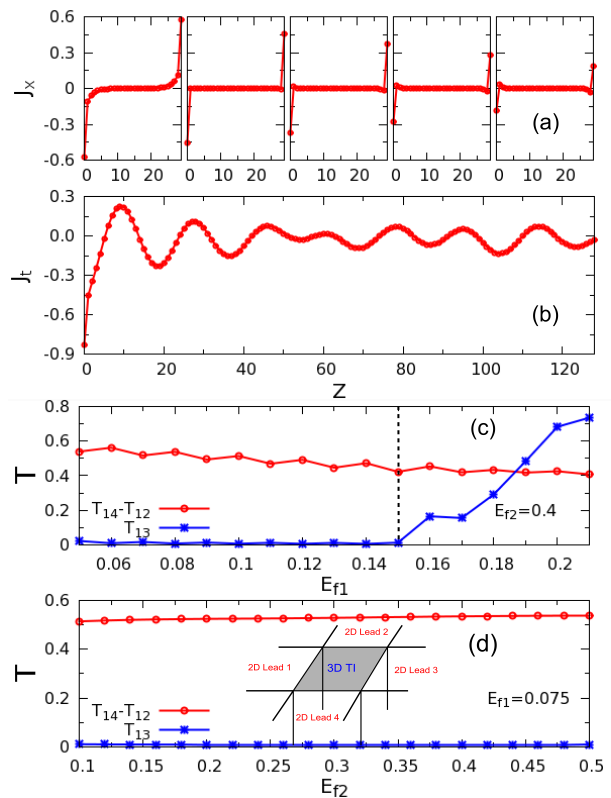


FIG. 4: (Color online) (a) Local current density J_x distribution along the width of Y ($L_y = 30a$) for the top 5 layers (the leftest is the 1st); (b) Total chiral current density J_t as a function of layer depth Z; (c) Transmission coefficients of the 4 terminal device, E_{f2} is fixed, the dashed line indicates the gap position; (d) same with (c), E_{f1} is fixed, the insert schematically illustrated the device set up. Other parameters are $\Delta_z = 0.15$, $M = 0.4$, $E_f = 0.075$.

After establishing the existence of the chiral surface-edge states, we calculate the Hall conductance numerically using the Landauer-Büttiker formalism [24–26]. The set up of the device is illustrated in the insert of the Fig. 4d: four 2D metallic leads ($\mu = 1, 2, 3, 4$) are attached to the top surface of a semi-infinite 3D topological insulator, acting as the measurement electrodes. The Zeeman field is normal to the top surface. The multi-terminal conductance can be deduced from the transmission coefficient T_{pq} from the terminal p to terminal q , $T_{pq} = \text{Tr}[\Gamma_p G^R \Gamma_q \Gamma^q]$ where Γ_p is determined by the self energy at the terminal p [25]. The calculated transmission coefficients as a function of chemical potentials E_{1f} in the 3D topological insulator and E_{2f} in the terminals are plotted in Figs. 4c and 4d. When the chemical potential E_{1f} is located in the gap of the surface states, the transmission coefficients show the "half chirality", i.e., $T_{pq} - T_{qp} \approx \pm 1/2$ between the two neighboring terminals p and q , and $T_{pq} = 0$ between the non-neighboring terminals. This is different from the chirality shown in the usual quantum Hall system, where $T_{pq} - T_{qp} = \pm 1$ between the two neighboring terminals. It is also important to note that the transmission coefficient between the two neighboring terminals could be very large due to the presence of the metallic side facets, and it is the difference between the clockwise and anti-clockwise transmission coefficients that shows the "half quantization".

The predicted half quantization can be directly measured. The straightforward way to observe it in the four-terminal setup is to apply a voltage between the terminals 1 and 3 (V_{13}), and measure the current between the terminal 2 and 4 (I_{24}). It is easy to show that the cross-conductance $\sigma_{24,13} \equiv I_{24}/V_{13} = (e^2/2h)(T_{12} - T_{21})$, yielding $e^2/4h$ for the half quantization. The measurement using the usual six-terminal Hall bar configuration could be more tricky due to the presence of the metallic side facets, which give rise to the finite longitudinal conductance σ_L . In the limit of thick sample with $\sigma_L \gg e^2/h$, the Hall conductance σ_H should approach to $(4e^2/h)(T_{12} - T_{21})$. It yields $2e^2/h$ for the half quantization. It can be distinguished from the usual quantized Hall effect by the finite longitudinal conductance.

To summarize, we find a chiral surface-edge state for a 3D topological insulator in the presence of Zeeman splitting. Effectively, one can consider that the original chiral edge mode carrying one conductance quantum e^2/h is split into two halves concentrated around the two boundaries between the insulating domains and metallic region. Its origin is quite different from those in integer quantum Hall and quantum spin Hall effect, in which there exist well defined chiral edge states. Here, many conducting channels, each contributing a fraction of the chirality, may give rise to an effective edge state concentrated around the domain boundaries, as indicated by the spatial distribution of the chiral edge current. The half quantization can be measured in the multi-terminal

setup. Moreover, the existence of the effective edge state may be directly observable. For example, because the spin polarization of Dirac fermions in the surface states is proportional to the charge current, the spatial oscillatory pattern of the chiral edge current associating with the effective edge state could be directly probed by the spatially resolved Kerr rotation technique [27].

The authors thank Z. Fang, Q. F. Sun, W. Yao and F. C. Zhang for helpful discussions. This work was supported by the Research Grant Council of Hong Kong under Grant No.: HKU 7037/08P, and HKUST3/CRF/09.

-
- [1] J. E. Moore, *Nature* **464**, 194 (2010).
 - [2] X. L. Qi and S. C. Zhang, *Phys. Today* **63**, 33 (2010)
 - [3] Z. Hasan and C. L. Kane, arXiv: 1002.3895
 - [4] L. Fu, C. L. Kane and E. J. Mele, *Phys. Rev. Lett.* **98**, 106803 (2007).
 - [5] J. E. Moore and L. Balents, *Phys. Rev. B* **75**, 121306 (2007).
 - [6] D. Hsieh, D. Qian, L. Wray, Y. Xia, Y. S. Hor, R. J. Cava and M. Z. Hasan, *Nature (London)* **452**, 970 (2008); D. Hsieh, Y. Xia, L. Wray, D. Qian, A. Pal, J. H. Dil, J. Osterwalder, F. Meier, G. Bihlmayer, C. L. Kane, Y. S. Hor, R. J. Cava, and M. Z. Hasan, *Science* **323**, 919 (2009)
 - [7] H. J. Zhang, C. X. Liu, X. L. Qi, X. Dai, Z. Fang and S. C. Zhang *Nature Physics* **5**, 438 (2009)
 - [8] Y. Xia, D. Qian, D. Hsieh, L. Wray, A. Pal, H. Lin, A. Bansil, D. Grauer, Y. S. Hor, R. J. Cava and M. Z. Hasan, *Nature Physics* **5**, 398 (2009)
 - [9] Y. L. Chen, J. G. Analytis, J. H. Chu, Z. K. Liu, S. K. Mo, X. L. Qi, H. J. Zhang, D. H. Lu, X. Dai, Z. Fang, S. C. Zhang, I. R. Fisher, Z. Hussain, and Z. X. Shen, *Science* **325**, 178 (2009)
 - [10] T. Yokoyama, Y. Tanaka and N. Nagaosa. *Phys. Rev. B* **81**, 121401(R) (2010)
 - [11] I. Garate, M. Franz. *Phys. Rev. Lett* **104**, 146802 (2010)
 - [12] A. N. Redlich, *Phys. Rev. D* **29**, 2366 (1984).
 - [13] R. Jackiw, *Phys. Rev. D* **29**, 2375 (1984); A. M. J. Schakel, *Phys. Rev. D* **43**, 1428 (1991).
 - [14] X. L. Qi, T. L. Hughes, and S. C. Zhang, *Phys. Rev. B* **78**, 195424 (2008)
 - [15] X. L. Qi, R. D. Li, J. D. Zang, and S. C. Zhang, *Science* **323**, 1184 (2009)
 - [16] A. M. Essin and J. E. Moore, *Phys. Rev. Lett.* **102**, 146805 (2009)
 - [17] B. I. Halperin, *Phys. Rev. B* **25**, 2185 (1982).
 - [18] A. H. MacDonald and P. Streda, *Phys. Rev. B* **29**, 1616 (1984).
 - [19] W. Y. Shan, H. Z. Lu, and S. Q. Shen, *New J. Phys.* **12**, 043048 (2010).
 - [20] H. Z. Lu, W. Y. Shan, W. Yao, Q. Niu and S. Q. Shen, *Phys. Rev. B* **81**, 115407 (2010)
 - [21] S. Murakami, *New J. Phys.* **9**, 356 (2007)
 - [22] M. P. L. Sancho, J. M. L. Sancho and J. Rubio, *J. Phys. F: Met. Phys.* **14**, 1205 (1984)
 - [23] C. Kittel, *Introduction to Solid State Physics*, (7th ed.) p 283 (John Wiley & Sons, New York, 1996)
 - [24] M. Buttiker, *Phys. Rev. Lett.* **57**, 1761 (1986).

- [25] S. Datta, *Electronic Transport in Mesoscopic Systems* Cambridge University Press, Cambridge, (1995).
- [26] J. Li, L. Hu, and S. Q. Shen, *Phys. Rev. B* **71**, 241305(R) (2005)
- [27] Y. K. Kato, R. C. Myers, A. C. Gossard, D. D. Awschalom, *Science* **306**, 1910 (2004).